



저작자표시-비영리-변경금지 2.0 대한민국

이용자는 아래의 조건을 따르는 경우에 한하여 자유롭게

- 이 저작물을 복제, 배포, 전송, 전시, 공연 및 방송할 수 있습니다.

다음과 같은 조건을 따라야 합니다:



저작자표시. 귀하는 원저작자를 표시하여야 합니다.



비영리. 귀하는 이 저작물을 영리 목적으로 이용할 수 없습니다.



변경금지. 귀하는 이 저작물을 개작, 변형 또는 가공할 수 없습니다.

- 귀하는, 이 저작물의 재이용이나 배포의 경우, 이 저작물에 적용된 이용허락조건을 명확하게 나타내어야 합니다.
- 저작권자로부터 별도의 허가를 받으면 이러한 조건들은 적용되지 않습니다.

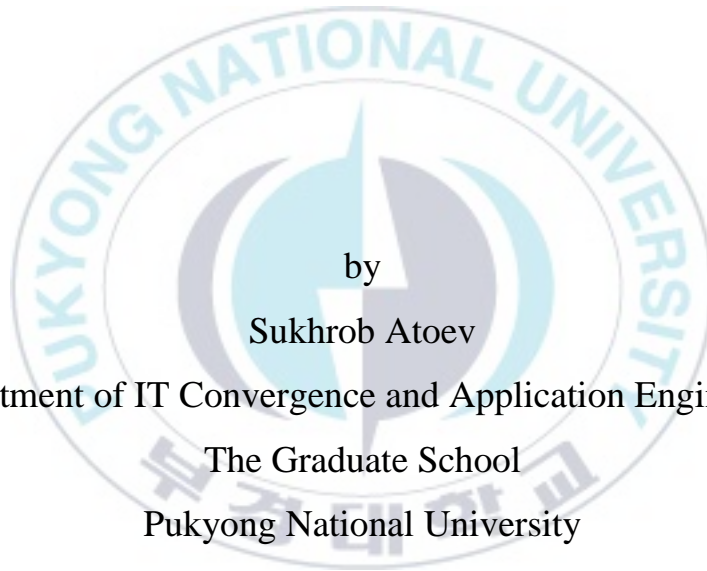
저작권법에 따른 이용자의 권리는 위의 내용에 의하여 영향을 받지 않습니다.

이것은 [이용허락규약\(Legal Code\)](#)을 이해하기 쉽게 요약한 것입니다.

[Disclaimer](#)

Thesis for the Degree of Master of Engineering

# An Efficient and Secure Communication Link for Unmanned Aerial Vehicle



February 2019

An Efficient and Secure Communication  
Link for Unmanned Aerial Vehicle  
무인 항공기를 위한 효율적이고  
안전한 통신 링크

Advisor: Prof. Ki-Ryong Kwon

by  
Sukhrob Atoev

A thesis submitted in partial fulfillment of requirements for  
the degree of

Master of Engineering

in Department of IT Convergence and Application Engineering  
The Graduate School, Pukyong National University

February 2019

An Efficient and Secure Communication Link for Unmanned  
Aerial Vehicle

A thesis

by

Sukhrob Atoev

Approved by:

  
\_\_\_\_\_  
(Chairman) Prof. Kwang-Seok Moon

  
\_\_\_\_\_  
(Member) Prof. Bong-Kee Sin

  
\_\_\_\_\_  
(Member) Prof. Ki-Ryong Kwon

February 2019

# Contents

<b>I. Introduction .....</b>	<b>1</b>
1.1 Unmanned Aerial Vehicle (UAV).....	1
1.2 UAV Applications.....	3
1.3 Outline of Thesis .....	3
<b>II. Related Works .....</b>	<b>5</b>
2.1 MAVLink Communication Protocol .....	5
2.1.1 Overview .....	5
2.1.2 Securing the MAVLink Communication Protocol .....	6
2.2 Improving Efficiency of the UAV Communication Link.....	8
2.2.1 UAV Communication System.....	8
2.2.2 UAV Transmitter .....	10
2.3 SC-FDM Modulation Technique .....	11
<b>III. The Proposed Methods and Results .....</b>	<b>14</b>
3.1 The Secure UAV Communication Link Based on AES-128 Encryption Algorithm.....	14
3.1.1 Data Analysis of MAVLink.....	14
3.1.1.1 Experimental Configuration .....	15
3.1.1.2 Result Analysis.....	16
3.1.2 AES Encryption Algorithm.....	17
3.1.3 Methodology .....	21
3.1.4 Experimental Results and Analysis.....	22

3.2	An Efficient SC-FDM Modulation Technique for a UAV Communication Link .....	25
3.2.1	The Proposed SC-FDM and OFDM .....	25
3.2.1.1	OFDM .....	26
3.2.1.2	SC-FDM .....	26
3.2.2	Experiments and Performance Measures .....	28
3.2.2.1	Experiments .....	28
3.2.2.2	Peak-to-Average Power Ratio (PAPR) .....	32
3.2.2.3	Bit Error Rate (BER) .....	33
3.2.2.4	Pulse Shaping .....	35
3.2.3	Results Analysis .....	37
3.2.3.1	The Impulse and Frequency Responses of the Raised-Cosine (RC) filter.....	37
3.2.3.2	PAPR Results .....	39
3.2.3.3	The Probability of Bit Error Results.....	42
<b>IV.</b>	<b>Conclusion .....</b>	<b>45</b>
	<b>References .....</b>	<b>46</b>
	<b>Acknowledgement .....</b>	<b>52</b>

# Figures

Fig. 1. DJI Phantom 4 Pro drone.....	1
Fig. 2. UAV applications.....	3
Fig. 3. Structure of the MAVLink packet. ....	5
Fig. 4. Communication link between MAV and GCS. ....	7
Fig. 5. UAV Communication Link.....	9
Fig. 6. UAV communication system components.....	10
Fig. 7. Block diagram of UAV transmitter.....	11
Fig. 8. Hardware architecture.....	12
Fig. 9. Overview of data analysis process.....	14
Fig. 10. Mission Planner software.....	15
Fig. 11. Average packet loss against distance.....	17
Fig. 12. The AES conceptual scheme. ....	18
Fig. 13. The AES-128 bit cipher.....	19
Fig. 14. The overall structure of the AES encryption algorithm.....	20
Fig. 15. System overview.....	21
Fig. 16. Securing the communication link. ....	22
Fig. 17. Accuracy comparison of different encryption algorithms. ....	23
Fig. 18. Execution time for different encryption algorithms.....	24
Fig. 19. OFDM and SC-FDM. ....	25
Fig. 20. Block diagram of SC-FDM modulation process.....	28
Fig. 21. Layout of experimental setup.....	29
Fig. 22. Mission Planner GCS: (a) Radio link status; (b) “Flight Data” screen.....	30
Fig. 23. The impulse and frequency responses of the RC filter: (a) The impulse response; (b) The frequency response.....	38
Fig. 24. The PAPR performances of SC-FDM and OFDM for M-ary PSK modulation schemes: (a) BPSK; (b) QPSK; (c) 8-PSK. ....	41

Fig. 25. The PAPR performances of SC-FDM and OFDM for M-ary QAM modulation schemes: (a) 16-QAM; (b) 64-QAM.....42

Fig. 26. The probability of bit error of different modulation schemes for SC-FDM modulation technique. ....43

Fig. 27. Computation time comparison of SC-FDM and OFDM. ....44



## Tables

Table 1. The measurements of average network latency and packet loss. ....	17
Table 2. Main control commands.....	23
Table 3. Accuracy of the different encryption algorithms. ....	24
Table 4. Simulation parameters.....	31
Table 5. PAPR results for SC-FDM and OFDM.....	42
Table 6. Computation time for SC-FDM and OFDM.....	44



# 무인 항공기를 위한 효율적이고 안전한 통신 링크

Sukhrob Atoev

부경대학교 대학원 IT 융합 응용 공학과

## 요 약

급속하게 발전하는 기술로 무인 항공기 (UAV)는 널리 알려져 있으며 최근 몇 년 동안 점점 더 효과적이고 비용이 많이 들지 않았습니다. 이 차량은 파일럿 운영자가 원격 제어 (RC)하거나 내장 컴퓨터로 자율적으로 제어 할 수 있습니다. UAV의 통신 링크와 신뢰성 평가는 힘든 분야이므로, 우리는이 주제에 대한 연구에 집중했습니다. UAV의 통신 및 데이터 링크의 타당성과 신뢰성에 대한 요구는 현대 전장의 환경이 점점 더 복잡해지고 있기 때문에 훨씬 더 높습니다. 따라서 차량과 지상 제어국 (GCS) 간의 통신 채널은 안전하고 효율적인 데이터 링크를 제공해야 합니다. 이 논문은 MAVLink 통신 프로토콜의 네트워크 대기 시간과 데이터 손실을 분석합니다. 이 논문에서는 Mission Planner 및 Wireshark 소프트웨어를 사용하여 GCS와 자동 조종간의 데이터 링크를 분석하기 위해 무인 항공기 대신 APM 2.8 보드가 사용되었습니다. 이 논문은 AES-128 암호화 알고리즘을 사용하여 MAVLink 프로토콜을 보호하는 방법을 제안한다. 또한, 다른 유형의 통신과 유사하게, UAV의 데이터 링크는 장거리 작동, 고효율, 신뢰성있는 통신 및 낮은 대기 시간과 같은 몇 가지 요구 사항을 가지고 있습니다. 효율적인 데이터 링크를 달성하려면 UAV의 비행 시간, 데이터 전송 속도 및 통신 링크의 신뢰성을 증가시키는 매우 효율적인 변조 기술을 채택해야 합니다. 이를 위해 우리는 UAV 통신 시스템을 위한 단일 캐리어 주파수 분할 다중화 (SC-FDM) 변조 기술을 연구했다. 비교 연구로부터 얻어진 결과는 SC-FDM이 UAV 통신 링크에 대해 현재 사용되는 변조 기술보다 우수한 성능을 나타냄을 보여준다.

# An Efficient and Secure Communication Link for Unmanned Aerial Vehicle

Sukhrob Atoev

Department of IT Convergence and Application Engineering,  
the Graduate School,  
Pukyong National University

## Abstract

With the rapidly advancing technology, unmanned aerial vehicles (UAVs), widely known as drones, are becoming increasingly effective and significantly less costly during the most recent years. These vehicles can be controlled either under remote control (RC) by a pilot operator or autonomously by onboard computers. Since the communication link of a UAV and its reliability evaluation represent an arduous field, we have concentrated our work on this topic. The demand on the validity and reliability of the communication and data link of a UAV is much higher since the environment of modern battlefield is becoming more and more complex. Therefore, the communication channel between the vehicle and ground control station (GCS) should be secure and provide an efficient data link. This thesis analyzes the network latency and data loss of the MAVLink communication protocol. In this thesis, APM 2.8 board was used instead of drone in order to analyze the data link between the GCS and autopilot using Mission Planner and Wireshark softwares. The thesis proposes a method of securing the MAVLink protocol using AES-128 encryption algorithm. Furthermore, similar to other types of communications, data link of a UAV has several requirements such as long range operation,

high efficiency, reliable communication and low latency. In order to achieve an efficient data link, we need to adopt a highly efficient modulation technique, which leads to an increase in flight time of the UAV, data transmission rate and reliability of communication link. For this purpose, we have investigated the single carrier frequency division multiplexing (SC-FDM) modulation technique for a UAV communication system. The results obtained from the comparative study demonstrate that SC-FDM has better performance than currently used modulation technique for a UAV communication link.



# I. Introduction

## 1.1 Unmanned Aerial Vehicle (UAV)

An Unmanned Aerial Vehicle (UAV) is a pilotless aerial vehicle that can be controlled either autonomously by onboard computers or remotely controlled by a pilot at the Ground Control Station (GCS). In our current society, UAVs also known as drones have become common (see Figure 1). A UAV communication channel is a key factor that can affect the performance of the data link in terms of high data rate and reliable transmission of information. In other words, ensuring the efficiency of a UAV communication link represents one of the great challenges of the current works regarding a UAV communication system.

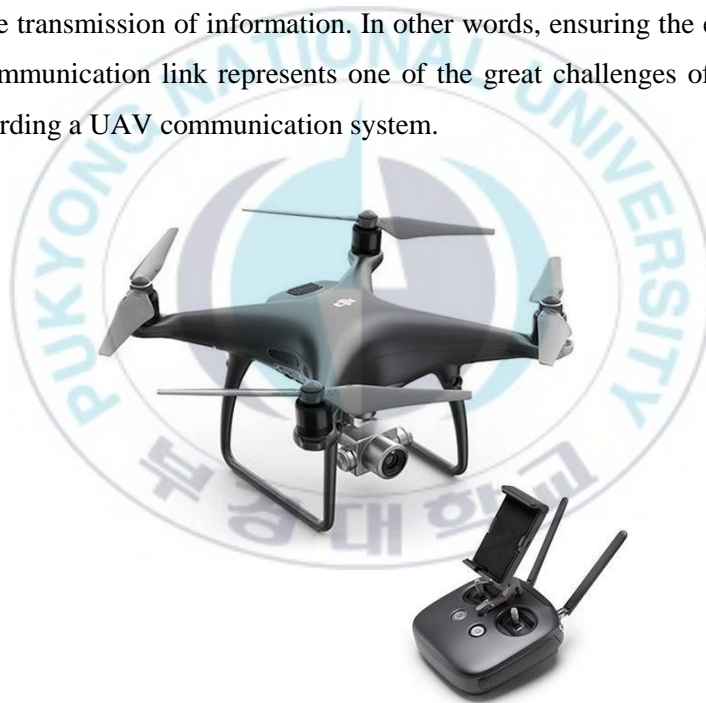


**Fig. 1.** DJI Phantom 4 Pro drone.

The UAV communication system has following major requirements:

- Efficient data link
- Long range operation

- Bidirectional communication
- Low latency
- Long flight time
- Operational capabilities
- Reliable communication

As the transmission of control commands and gathered data, which can be the recorded video and photo, is achieved through the communication channel between the UAV and the ground control station (GCS), UAV data link requires the highest reliability in data transmission as well as high data transfer rate. Nowadays, in order to provide an efficient communication link, many drones use the spread spectrum technology that allows many different pilots to operate in the same 2.4 GHz band without conflicts. Receivers in this band are virtually immune against interference issues.

Essentially, two types of spread spectrum technology are used for the UAV communication link. The first one is the frequency-hopping spread spectrum (FHSS), which unceasingly changes its narrow band frequency on several occasions a second within the 2.4 GHz frequency range. In this process, the receiver recognizes the patterns of frequency that are utilized by a transmitter. Because the transmitter changes frequency from one to another, the receiver can adopt the suitable frequency. Unlike FHSS, direct-sequence spread spectrum (DSSS) system uses a much wider bandwidth to transmit the signal on a single selected frequency. The transmitter sends original narrow band signal via a spreading code generator that multiplies the narrow band data signal using a much higher frequency. Anyway, both spread spectrum modes transmit the signal within the 2.4 GHz frequency band. In practice, orthogonal frequency division multiplexing (OFDM) modulation has been considered more efficient than FHSS and DSSS due to its greater tolerance of multipath distortion, higher throughput and potential data rate [1].

## 1.2 UAV Applications

Nowadays, UAVs have either been considered for or have seen limited utilization in a wide range of applications that include but are not limited to power line inspection; ship inspection; mine inspection; dam inspection; anomaly detection/prevention; early fire detection and forest protection; hazard monitoring; traffic monitoring; environmental monitoring; delivery services; military tasks; search and rescue operations; emergency response; border patrol; harbor patrol; police surveillance; aerial photography; imaging and mapping; intelligence, surveillance, and reconnaissance (ISR); chemical spraying; crop dusting; night vision; and entertainment industry and filming [2, 3].



Fig. 2. UAV applications.

## 1.3 Outline of Thesis

UAVs have a radio that enables wireless communication with a GCS or a remote control. In particular, the wireless communication channel opens up the door for several types of remote attacks. In this case, data link should be secure and it has to provide the low network latency [4]. For this purpose, we have provided a method to secure the UAV communication link using AES-128 encryption algorithm.

Nowadays, the demand on the long range operation and long flight time is increasing in UAV communication systems and the currently used modulation techniques have the fundamental constraint to meet this demand. Therefore, we need to adopt a potential modulation technique that fulfills this demand. In fact, it is essential to adopt the most effective technique that can provide a highly efficient data link between the vehicle and GCS. In this thesis, we have proposed the SC-FDM modulation technique in UAV communication system in order to provide an efficient UAV communication link and extend the flight time (battery life) of drones [5]. The performance of the adopted modulation technique is analyzed by comparing it with the OFDM modulation. Additionally, SC-FDM has been considered to transfer the data using different kinds of modulation schemes such as M-ary phase-shift keying (BPSK, QPSK and 8-PSK) and M-ary quadrature amplitude modulation (16-QAM and 64-QAM) in this work.

The remaining part of this thesis is structured as follows. In Section II, some related works and background theories are discussed. Section III presents the data analysis of the MAVLink communication protocol; our proposed method to secure the UAV communication link using AES-128 encryption algorithm; comparison of proposed SC-FDM modulation technique and OFDM modulation; experimental setup, performance measures of the system and results. At the end of the paper, Section IV illustrates our conclusions and some future works.

## II. Related Works

### 2.1 MAVLink Communication Protocol

#### 2.1.1 Overview

The Micro Air Vehicle Link Communication Protocol allows entities to communicate over a wireless channel. When used in drones, it is used for the bidirectional communications between the drone and the GCS. The GCS sends commands and controls to the drone whereas the drone sends telemetry and status information [6]. MAVLink was first released early 2009 by Lorenz Meier under Lesser General Public License for real time applications [7]. This protocol has been extensively tested on several UAV platforms, and numerous GCS software applications that run on Microsoft Windows, Mac and Linux OSs.

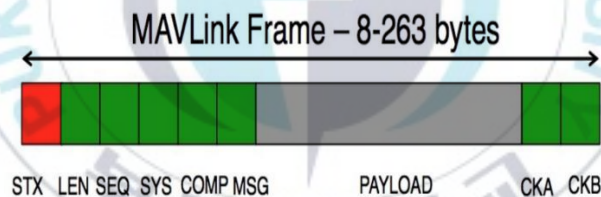


**Fig. 3.** Structure of the MAVLink packet.

There are 18 message types in the MAVLink protocol, and 91 defined messages in the MAVLink documentation. The message types establish encoding parameters such as architecture types, configuration settings and command message type (e.g., autopilot hardware, vehicle type, command for servo, etc.) designated by the message ID, so the receiving device will be able to properly decode the message payload. For this reason, the message type is the first field of the MAVLink message. The MAVLink messages carry the commands transmitted from the GCS to the UAV,

and provide feedback (e.g., telemetry, heartbeat, and system status) from the UAV to the GCS, enabling the pilot to maintain control of the aircraft. These messages are sent as data packets between the ground station and autopilot to properly fly the UAV [8]. MAVLink can support up to 255 aircraft being controlled by one GCS. The minimum packet length in the MAVLink protocol is 8 bytes (e.g., Acknowledgement (ACK) with no payload), and the maximum packet length is 263 bytes with a full payload. Figure 3 shows the structure of the MAVLink packet.

A bidirectional link is necessary to transmit control and telemetry data. Telemetry data will be sent from the aerial vehicle to the GCS, and control data will take the opposite way [9]. A MAVLink message is sent bitwise over the communication channel, followed by a checksum for error correction. If the checksum does not match, then it means that the message is corrupted and will be discarded. MAVLink uses a packet start sign (STX) to sync the start of an encoded message. Once the packet start sign is received, the packet length ( $n$ ) is read and after  $n$  bytes the checksum (CKA and CKB) is verified. If the checksum matches, the decoded packet is processed, an ACK message is transmitted, and it awaits the next start sign. Altered or lost message bytes will result in a checksum failure causing the packet to be dropped, and the receiving device resumes listening for the next start sign packet. MAVLink uses a sequence number (SEQ) for each packet as a safety mechanism to monitor packet loss detection. If the packet loss rate appears to be significant, the pilot would command the UAV to return to launch or at least reduce the operating range.

### **2.1.2 Securing the MAVLink Communication Protocol**

Based on the sensitivity of the mission there is a necessity to protect the data while transmission [10]. Encryption of the data being transmitted is one of the widely adapted techniques for data protection. Several encryption schemes are available in the literature. DES, AES, Blowfish, FEAL, IDEA, SAFER, RC5 etc. are some of

frequently used symmetric encryption algorithms. In [11], the authors present a comparative study of these algorithms and concludes that AES is best in terms of guaranteed security. This has become the standard for encryption to protect sensitive information by all U.S. government organizations on May 26, 2002 [13].

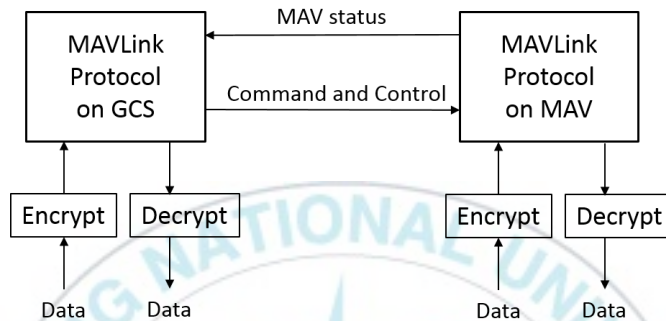


**Fig. 4.** Communication link between MAV and GCS [12].

The encryption algorithm uses a key or a password to encrypt/decrypt the data. This key is shared between two MAVs for secure data transmission. Key sharing is also an important aspect to be considered. Further, an authentication mechanism is required to ensure the data transfer to intended target. A communication link between MAV and the GCS is established using a predefined communication protocol MAVLink [7] is a widely used open source protocol. In [14], the encryption scheme chosen to realize a secure communication link for information transfer between a MAV and its GCS. The scheme involves AES-128 in CTR mode for encryption, SHA-256 for key hashing and Diffie Hellman algorithm for key exchange. This scheme is developed both on the MAV autopilot and the GCS and integrated with the MAVLink protocol. The feasibility study was carried out on MATLAB and found to be successful. This encryption and authentication method is not only useful for MAVData, further it can be extended for control or command messages and parameter messages [13].

## **2.2 Improving Efficiency of the UAV Communication Link**

A method for improving efficiency of the UAV communication link can be found in [7]. In this work, the key tasks of a UAV communication system and characteristics of radio channel between the UAV and ground control unit (GCU) have been analyzed. Considering the various issues of a UAV communication link, an author proposed the optimal way of radio channel construction using the rotary and mounting platform with antennas, power and low noise amplifiers as well as OFDM modulation technique to increase the data transfer rate. In [8], Wu et al. proposed OFDM as a transmission system for UAV wireless communications. Initially, to find out the proper OFDM system parameters, the coherence time and Doppler spread have been measured. After obtaining the inter carrier interference (ICI) coefficients, they evaluated the BER performance of OFDM technology in a typical UAV communication channel and these performance results were compared with those of OFDM in normal wireless indoor channels. According to their simulation results, an insignificant performance degradation can be seen when the OFDM technology is applied to the UAV communication channel.

### **2.2.1 UAV Communication System**

In general, a UAV communication link can both send control commands from the GCS to vehicle and receive data about the flight on downlink, as shown in Figure 5. A bidirectional link can be established in order to provide a communication between the drone and GCS [23]. A communication link between these two components has to provide long range operations as well as a continuous and stable link. Therefore, the establishment of a channel model that is suitable for UAV characteristics plays an important role in improving the data link of a UAV [24, 25]. Furthermore, for improving reliability of the data link, an adaptive information rate method is presented in [26].

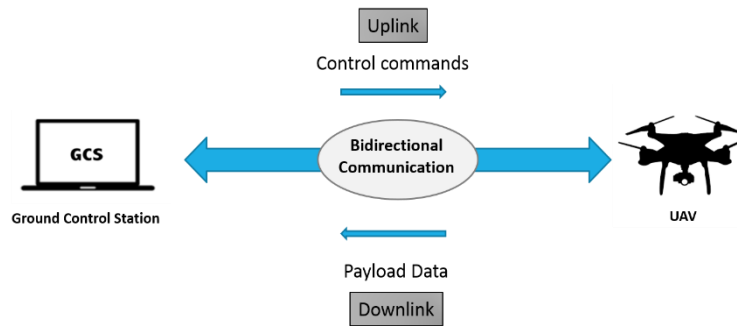


**Fig. 5.** UAV Communication Link.

Figure 6 illustrates the components of the UAV communication system. The main component is the microcontroller, also referred as flight controller, which is the core for all functioning of a UAV. It manages failsafe, autopilot, waypoints and many other autonomous functions. This microcontroller interprets input from receiver, global positioning system (GPS) module, battery monitor, inertial measurement unit (IMU) that include accelerometer and gyroscope which can be used for providing stability or maintain a reference direction in navigation system [27] and other onboard sensors. The GCS provides relevant data about the vehicle such as speed, attitude, altitude, location, yaw, pitch, roll, warnings and other information [28]. As shown in Figure 6, a UAV has two links: data link and communication link. To ensure the transmission of data between the vehicle and GCS, a UAV uses a data link that operates in the frequency range from 150 MHz to 1.5 GHz. On the other hand, a 2.4 GHz frequency band that determines the communication link between the transmitter and receiver is used in order to control the vehicle.

It should be noted that the transmitter and receiver must both be on the same frequency. In point of fact, drones have exclusive use of their own frequency allocation due to the longer range and potentially worse consequences of radio interference. Initially, drones scan the range of frequencies within the 2.4 GHz band and use only the narrow band frequency that is not in use by another drone. As a

result of that, many drones can utilize a 2.4 GHz frequency band simultaneously. This feature of drones can be noticeable when the number of drones are used as flying base stations in wireless cellular networks to serve an arbitrarily located set of users [29-31]. Moreover, typical UAVs use multiple radio interfaces to maintain continuous connection with essential links to GCSs, other UAVs and satellite relays.

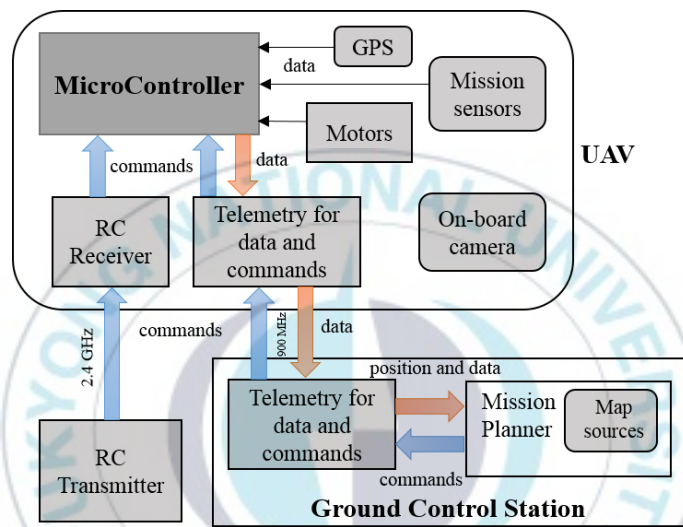
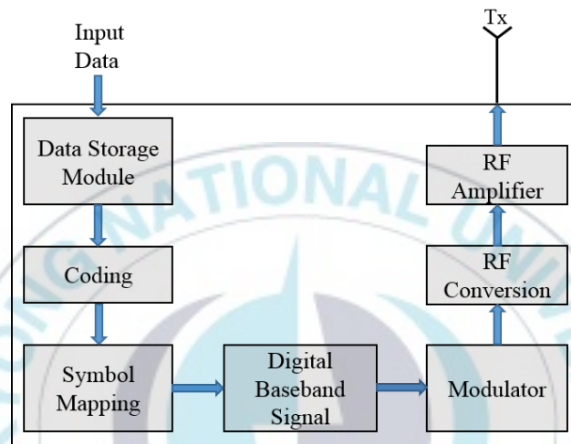


Fig. 6. UAV communication system components.

### 2.2.2 UAV Transmitter

The modulation and demodulation process of transmitted signal through a wireless channel can respectively be done in the transmitter and receiver of the UAV communication system. Figure 7 shows the typical transmitter of a UAV communication system that transmits the control commands and telemetry data. Initially, the input data is stored on data storage module, then, the channel coding can be used for error correction encoding. After that, the data streams are mapped into the frames and ready for channel modulation. The baseband modulation of each carrier can be selected among BPSK, QPSK, 8-PSK, 16-QAM and 64-QAM

depending on the channel condition. The modulated signals are then directly converted into the radio frequency band for wireless transmission. Before transmitting a signal, the radio frequency (RF) amplifier can be used to convert a low-power frequency signal into a higher one. Finally, the RF signal transmission is done at the transmitter antenna.



**Fig. 7.** Block diagram of UAV transmitter.

### 2.3 SC-FDM Modulation Technique

In UAV applications, there have been few efforts to adopt the SC-FDM modulation technology for a UAV communication system, while it has been widely accepted in mobile communications. In [9], Miko and Nemeth proposed a hardware architecture which includes a Xilinx field-programmable gate array (FPGA) combined with the software-defined radio (SDR) chip and SC-FDM modulation system to provide a high data transmission rate and radio navigation for the communication link of UAV systems. Their proposed hardware design of the transceiver is shown in Figure 8. They implemented modulation, demodulation and coding functions in the FPGA. However, there is no indication of the performance of SC-FDM modulation in their work.

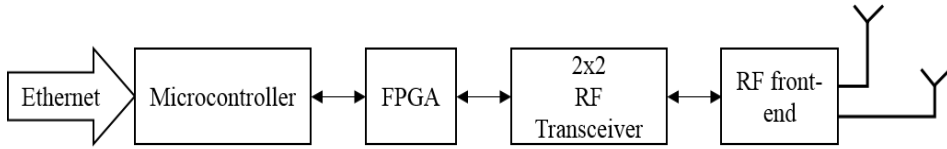


**Fig. 8.** Hardware architecture.

Until now, most of the previous works on the single carrier frequency division multiple access (SC-FDMA) have been done for uplink communications in the long term evolution (LTE) technology of mobile communication systems [10-15]. As an alternative to the orthogonal frequency division multiple access (OFDMA), SC-FDMA has drawn considerable attention in mobile communications. In [16], Myung gives an overview of SC-FDMA. Another research focuses on PAPR reduction of localized SC-FDMA using partial transmit sequence (PTS) [17]. Actually, there can be localized and distributed modes of subcarrier mapping in SC-FDMA [16, 18]. In localized SC-FDMA, each terminal uses a set of contiguous subcarriers for the transmission of symbols, thereby limiting them to only a portion of the system bandwidth. On the other hand, the subcarriers used by the terminal are propagated throughout the entire bandwidth in the distributed SC-FDMA. Localized SC-FDMA, which is used for uplink transmission of LTE systems, has lower PAPR than distributed SC-FDMA.

Furthermore, Tsiropoulou et al. [19] provided a bargaining model and power optimization framework to solve the problem of subcarrier and power allocation in multiuser SC-FDMA wireless networks. The obtained numerical results and key features of their proposed approach demonstrate that the introduced framework can be a foundation for the supporting heterogeneous services and the implementation of different users' priorities to access the available resources. Towards this direction, a similar work can be found in [20]. In 2016, Tsiropoulou et al. [21] studied and examined the various state-of-the-art resource allocation algorithms and frameworks developed to allocate the subcarriers and transmission power of users in the uplink

of SC-FDMA wireless networks. Luo and Xiong [22] proposed the SC-FDMA-IDMA system model, which is the combination of SC-FDMA and interleaved division multiple access (IDMA), and studied the effect of carrier frequency offset (CFO) on the BER performance of this system model.



### III. The Proposed Methods and Results

#### 3.1 The Secure UAV Communication Link Based on AES-128 Encryption Algorithm

##### 3.1.1 Data Analysis of MAVLink

In this research, APM 2.8 was used instead of drone in order to analyze the data link between the GCS and autopilot using Mission Planner and Wireshark softwares. A communication link between the APM and the GCS is established using a MAVLink communication protocol [24].

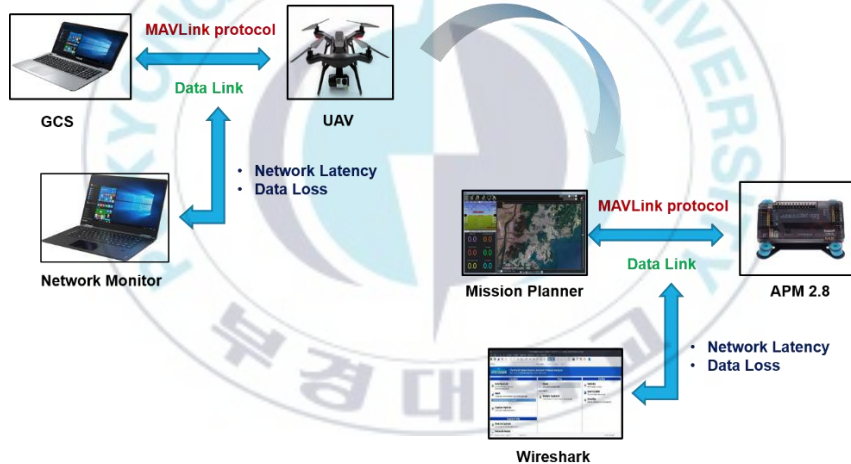


Fig. 9. Overview of data analysis process.

The APM 2.8 is a complete open source autopilot system that allows the user to turn any fixed, rotary wing or multicopter vehicle into a fully autonomous vehicle; capable of performing programmed GPS missions with waypoints. This revision of the board has no onboard compass, which is designed for vehicles (especially multicopters and rovers) where the compass should be placed as far from power and motor sources as possible to avoid magnetic interference. APM 2.8 features:

- Simple setup process and firmware loading via a point-and-click utility;
- Full mission scripting with point-and-click desktop utilities;
- Two-way telemetry and in-flight command using the powerful MAVLink protocol;
- Includes 3-axis gyro, accelerometer and magnetometer, along with a high-performance barometer;
- Onboard 4 MegaByte Dataflash chip for automatic datalogging;
- Optional off-board GPS, uBlox LEA-6H module with Compass;
- Barometric pressure sensor upgraded to MS5611-01BA03;
- ATMEGA2560 and ATMEGA32U-2 chips for processing and USB functions respectively.

### 3.1.1.1 Experimental Configuration

The MAVLink protocol is a way for users to maintain a connection to the APM when it is actually flying as though it was connected to the PC via the USB cable to control the APM by using Mission Planner software.

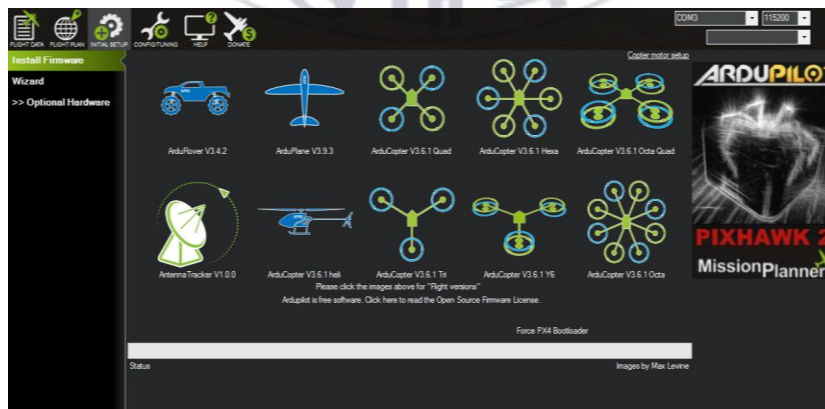


**Fig. 10.** Mission Planner software.

3DR 915 MHz Telemetry Radio is connected to the PC using a USB cable to setup a telemetry connection between the APM and GCS and it is easily done over the wireless link. The radio uses open source firmware which has been specially designed to work well with MAVLink packets and to be integrated with the Mission Planner, Copter, Rover and Plane. The radio has interchangeable air and ground modules, meaning that we can use them as a pair but it does not matter which one goes on the vehicle and which remains on the ground. Because of the limited number of serial ports on the APM2.8, the telemetry radio cannot be used while the board is also plugged in with the micro USB port. So, the actual elements that we need as we have kind of described a little bit already is on one side we have the APM 2.8 is going to install and the telemetry radio can be plugged into the this autopilot. We just make sure that the pin outs are same. After that, the ground is connected to ground, +5 volts is connected to the +5 volts and then obviously the transmitter is connected to receiver and the receiver is connected to the transmitter. Actually, these two wires are swapped. Finally, the telemetry radio is powered from the APM 2.8. On the other hand, second telemetry radio connected to the Mission Planner which is running on Windows PC. Connecting the radio to Windows PC is as simple as connecting the micro USB cable.

#### **3.1.1.2 Result Analysis**

The APM 2.8 autopilot module in this thesis was configured to analyze the network latency and data loss between the GCS and autopilot. Mission Planner supports configuring telemetry radios using a simple GUI interface. Wireshark software was used to capture and analyze the packets transmitted over the data link. The measurements of average network latency and packet loss of the MAVLink communication protocol during the each attempt are provided in Table 1.

**Table 1.** The measurements of average network latency and packet loss.

Distance between APM and GCS (meters)	Average Network Latency (seconds)	Average Packet Loss (%)
5m	0.17 sec	0.19
10m	0.25 sec	0.31
20m	0.42 sec	0.63

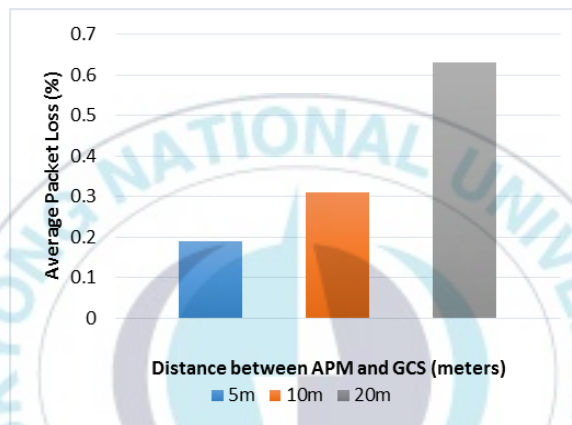


**Fig. 11.** Average packet loss against distance.

From the results shown above, we can see that the latency value varies greatly depending on the range of the autopilot from the system used for measurements, and on the configuration settings selected on the 3DR radios.

### 3.1.2 AES Encryption Algorithm

The Advanced Encryption Standard (AES), also known as Rijndael, is a symmetric block cipher chosen by the U.S. government to protect classified information and is implemented in software and hardware throughout the world to encrypt sensitive data. AES comprises three block ciphers: AES-128, AES-192 and AES-256. Each cipher encrypts and decrypts data in blocks of 128 bits using cryptographic keys of 128-, 192- and 256-bits, respectively, as shown in Figure 12.

Like nearly all encryption algorithms, AES relies on the use of keys during the encryption and decryption process. Since the AES algorithm is symmetric, the same key is used for both encryption and decryption.

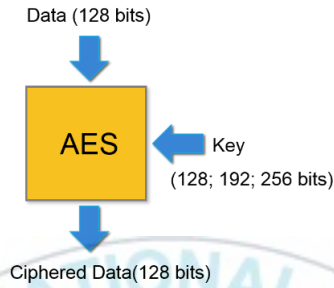


**Fig. 12.** The AES conceptual scheme.

The AES encryption algorithm defines a number of transformations that are to be performed on data stored in a 4 x 4 array of bytes  $b_{mn}$ , arranged in the matrix  $A$  as follows:

$$A = \begin{bmatrix} b_{00} & b_{01} & b_{02} & b_{03} \\ b_{10} & b_{11} & b_{12} & b_{13} \\ b_{20} & b_{21} & b_{22} & b_{23} \\ b_{30} & b_{31} & b_{32} & b_{33} \end{bmatrix} \quad (1)$$

The first step of the cipher is to put the data into a 4 x 4 array of bytes  $b_{mn}$ ; after which the cipher transformations are repeated over a number of encryption rounds. The number of rounds is determined by the key length, with 10 rounds for 128-bit keys, 12 rounds for 192-bit keys and 14 rounds for 256-bit keys [42].

In the AES, each byte is regarded as an element  $K$  of the finite field  $F_{2^8}$ , as expressed by the following equation:

$$K = \frac{F_2[x]}{\langle f(x) \rangle} \cong F_{2^8}, \quad (2)$$

where  $f(x) \in F_2[x]$  is the irreducible polynomial  $x^8 + x^4 + x^3 + x + 1$ .

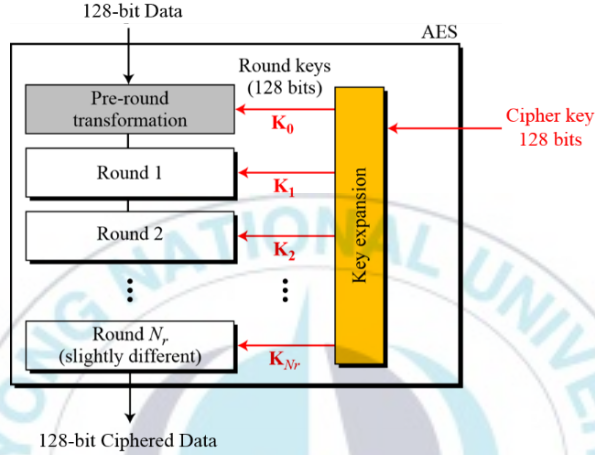


**Fig. 13.** The AES-128 bit cipher.

In this thesis, we have used the AES-128 bit cipher (see Figure 13) that can generate  $2^{128} = 3.4 \times 10^{38}$  possible keys to encrypt and decrypt the telemetry data that were collected from the GCS.

As illustrated in Figure 14, the input  $W$  is mapped to  $x = W^{(-1)}$ , where  $W^{(-1)}$  is defined by:

$$W^{(-1)} = W^{254} = \begin{cases} W^{-1}, & W \neq 0 \\ 0, & W = 0 \end{cases} \quad (3)$$

The general description of the AES algorithm is structured as follows:

- Key expansion:

- Round keys are derived from the cipher key using Rijndael's key schedule.
- Initial round:
  - AddRoundKey: each byte of the state is combined with the round key using bitwise XOR.
- Rounds:
  - SubBytes: non-linear substitution step;
  - ShiftRows: transposition step;
  - MixColumns: mixing operation of each column;
  - AddRoundKey: each byte of the state is combined with the round key using bitwise XOR.
- Final round:
  - SubBytes: non-linear substitution step;
  - ShiftRows: transposition step;
  - AddRoundKey: each byte of the state is combined with the round key using bitwise XOR.

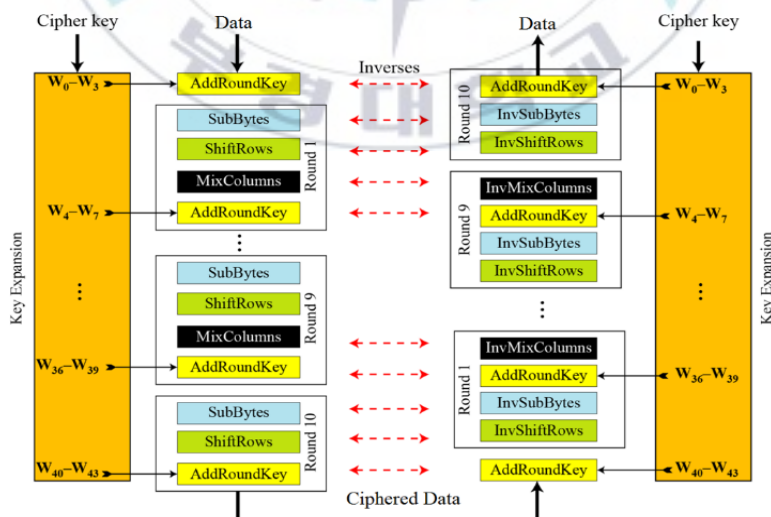


Fig. 14. The overall structure of the AES encryption algorithm.

### 3.1.3 Methodology

The secure UAV communication system, as shown in Figure 15, consists of the GCS, the UAV, an attacker, MAVLink protocol, and the data link used to facilitate communication. The GCS transmits commands to the UAV at a fixed interval to perform the legitimate command and control. The maximum command period is constrained by the latency of the UAV response to commands. The GCS remains idle listening for a response from the UAV before issuing a new command, followed by a pause sufficient to allow execution of the current command.

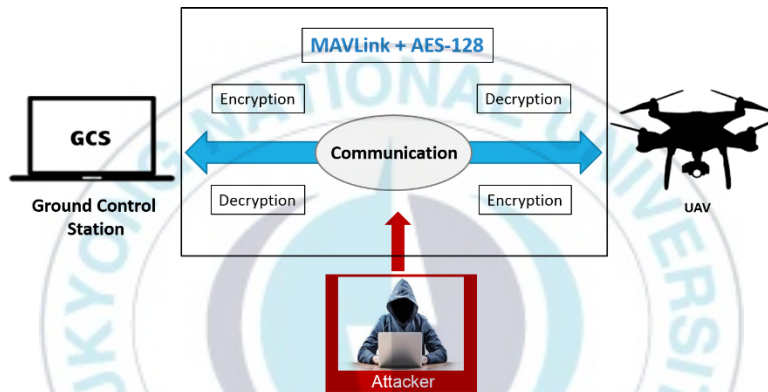


Fig. 15. System overview.

In the field, the command period of the GCS is dependent upon weather conditions affecting the UAV being tested because the next command is not transmitted until the UAV telemetry indicates successful completion of the current command. The data link interface is the peripheral input/output (IO) device that the GCS and the UAV must use to transmit and receive the messages over the data link. Each interface directly affects the network load metric, and the radio on board the

UAV also affects the power consumption metric. During the experiment, we have used two 3DR 915 MHz radios to communicate over the data link.

As presented in Figure 16, in order to secure the communication link, we have divided our work into two parts. In the first part, to secure the MAVLink protocol with AES-128 encryption algorithm, GCS source code was modified to include the encryption and decryption functions. In this step, we used the Mission Planner software as the GCS.



**Fig. 16.** Securing the communication link.

Secondly, in the same scenario, to secure the communication link between the drone and GCS, MAVLink protocol source code was modified to include the encryption and decryption functions.

### 3.1.4 Experimental Results and Analysis

In this thesis, the Java code is performed to encrypt and decrypt the data that can be the control commands, recorded videos and photos, which transmitted between the vehicle and GCS. There are several commands to control the UAV such as “Start-Engines”, “Auto-Takeoff”, “Enable Autopilot”, etc., in UAV communication

system. It should be mentioned that these control commands are represented by hexadecimal numbers as shown in Table 2.

**Table 2.** Main control commands.

Name	Hexadecimal numbers
Start-Engines	24 57 49 46 49 89 89 89
Auto-Takeoff	24 57 49 46 49 58 58 58
Enable Autopilot	24 57 49 46 49 97 97 97

$$Accuracy = \frac{\text{Number of encrypted bits}}{\text{Number of total bits}} \quad (4)$$

Accuracy of the different encryption algorithms is computed by using Equation (4) and shown in Figure 17 and Table 3. It can be observed that AES-128 algorithm encrypts and decrypts the data more accurately compare to 3DES, Twofish and OTP encryption algorithms.

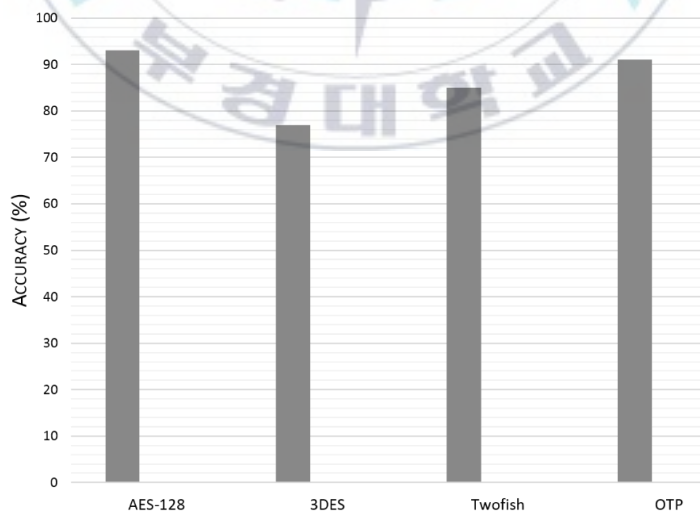


**Fig. 17.** Accuracy comparison of different encryption algorithms.

**Table 3.** Accuracy of the different encryption algorithms.

Encryption algorithm	Accuracy (%)
AES-128	93
3DES	77
Twofish	85
OTP	91

As demonstrated in Figure 18, the execution time for various encryption algorithms depends on the size of the data that can be the control commands, recorded videos and photos.

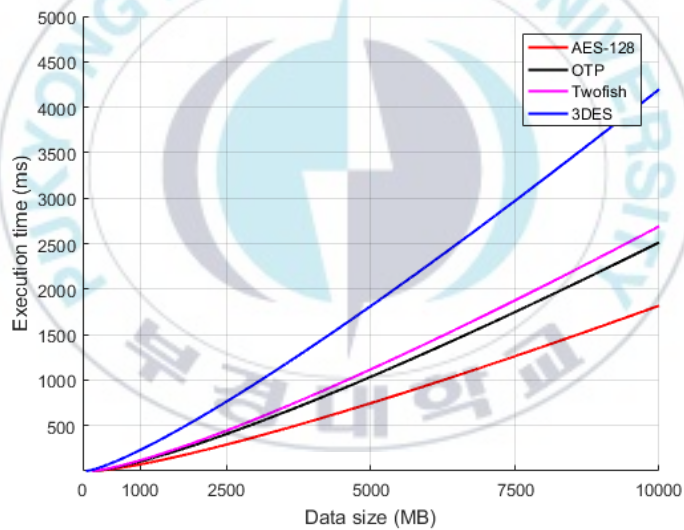


**Fig. 18.** Execution time for different encryption algorithms.

According to the accuracy and execution time performances that are presented in Figures 17 and 18, AES-128 is more effective than other encryption algorithms to secure the UAV communication link.

## 3.2 An Efficient SC-FDM Modulation Technique for a UAV Communication Link

### 3.2.1 The Proposed SC-FDM and OFDM

In general, SC-FDM behaves like a single carrier system with short symbol duration compared to OFDM. To achieve this, SC-FDM introduces an N-point DFT block right after the serial to parallel converter in the OFDM structure. The DFT block converts parallel sequences of symbols in time domain to different frequency points. The major disadvantage of the OFDM is its high PAPR. This is a consequence of the fact that the transferred signal is the amount of all the modulated subcarriers and some of them are in a phase with high amplitudes that cannot be avoided [32]. Due to this reason, the power structure of the transmitter is characterized by relatively low average and high power peaks.

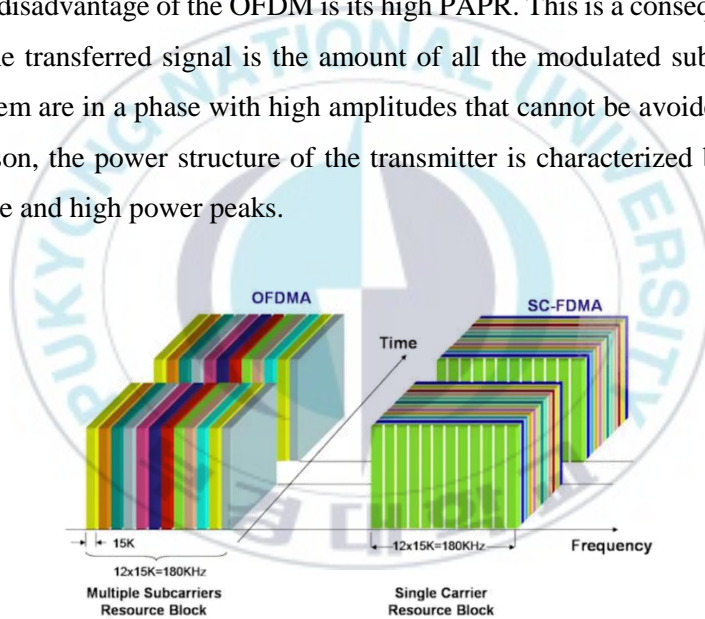


**Fig. 19.** OFDM and SC-FDM.

SC-FDM allows a symbol to be transmitted in parts over multiple subcarriers, but in OFDM, we have one to one mapping between symbol and subcarrier. For example, in OFDM one symbol occupies one subcarrier of 15 kHz, but in SC-FDM, same symbol is distributed among multiple subcarriers of 15 kHz, as described in Figure 19 [33].

### **3.2.1.1 OFDM**

As shown in Figure 19, the data can be transferred by parallel subcarriers of 15 kHz in OFDM. On the time axis, the further divided subcarriers represent blocks of one symbol duration. This basic unit is known as resource element and one symbol is carried by one resource element. In addition, the number of resource elements are used to make a resource block that is the basic unit of scheduling.

At the beginning of the modulation process, the data is modulated by particular modulation scheme in order to transfer the data over these resource elements. This modulation scheme depends on the physical channels mapped on the resource grid. Then, M-point IDFT transforms the signals of the parallel frequency domain into samples of a composite time domain signal, which are much easier to generate at transmitter side. All we need to do is to send these time domain samples at radio frequencies. In wireless channel due to multipath propagation, there can be delay spread and inter symbol interference (ISI) [34]. This interference may cause a given transmitted symbol to be distorted by other transmitted symbols. Since OFDM uses composite IDFT samples, cyclic prefix is added by taking some samples from the end of a symbol period, and placing them at the beginning. It provides orthogonality between the subcarriers by keeping the OFDM symbol periodic in the duration of the extended symbol and for that reason, avoiding intercarrier and interchannel interference simultaneously. In the next step, sampled signal is converted into an analog wave by a digital to analog converter (DAC). Further composite waveform is modulated at the desired RF for transmission. The noticeable advantage of OFDM over SC-FDM is that frequency domain representation of signals simplifies the signal error correction at the receiver [35].

### **3.2.1.2 SC-FDM**

SC-FDM is a hybrid modulation technique that combines the frequency allocation flexibility and multipath resistance of OFDM and other important characteristics of

a single carrier system. The crucial characteristic of the SC-FDM signal generation is that the PAPR of finite frequency shifted signal ends up being the same as that of the original modulating data symbols and this is very different from that of OFDM for the same occupied bandwidth in the same data rate. However, if the channel bandwidth is wider, the link between the symbol length and channel bandwidth can be considered as the disadvantage of SC-FDM in comparison with OFDM [35].

Figure 20 presents the block diagram for signal processing chain of SC-FDM. The first step is the same as for OFDM, modulating the data with one of the modulation schemes for data transmission over the resource elements. The data is placed over the resource elements by adjusting the phase and amplitude of subcarrier to those derived for the data stream. Mathematically, it means multiplying the complex modulation symbol to the corresponding subcarrier frequency. After this process, there is another block in the signal processing chain. To convert the data symbols from the time domain into the frequency domain, the DFT is performed after the serial to parallel conversion. As an OFDM, afterwards, there is subcarrier mapping and an IDFT to transform the signal in frequency domain into the time domain signal. The cyclic prefix can be inserted when the parallel to serial conversion is done. Before modulating the signal with high frequency, pulse shaping filter can be used to get the desired spectrum [36]. The original values of the symbols can be completely recovered if the transmitted signal is properly sampled at the receiver. The last two steps are the same as for OFDM. Thus, there is no difference in the downlink signal generation chain. In the same way, the reverse of what was done at the transmitter can be accomplished at the receiver. As mentioned in Section 4.1, each subcarrier carries only one particular modulation symbol in OFDM, while the DFT takes a symbol and spreads it via an available subcarrier in SC-FDM. For that reason, SC-FDM is also referred as DFT spread OFDM [37]. Since the PAPR is proportional to the square of the number of subcarriers involved, SC-FDM reduces the PAPR by reducing the number of subcarriers.

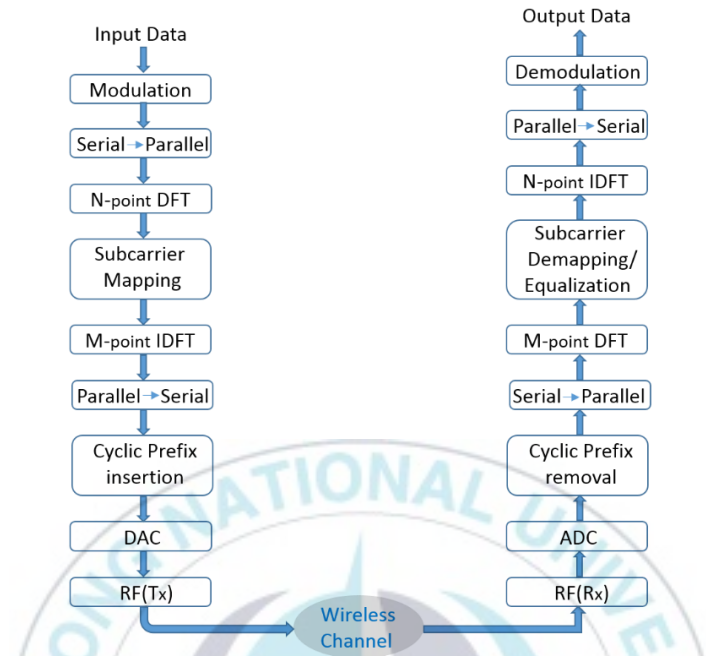


Fig. 20. Block diagram of SC-FDM modulation process.

### 3.2.2 Experiments and Performance Measures

#### 3.2.2.1 Experiments

In this section, we have performed the experimental setup by using the ArduPilot Mega (APM) 2.8 microcontroller and Mission Planner, which is the suitable GCS application for this microcontroller. The APM 2.8 microcontroller uses the micro air vehicle link (MAVLink) protocol [38] to maintain a connection between the APM 2.8 and GCS. During our experiments, the APM 2.8 board was tested instead of drone in order to obtain the flight data that were used to analyze the SC-FDM modulation for a UAV communication system. In our work, two 3DR 915 MHz telemetry radios were used to provide a data link. To setup a connection between the APM 2.8 and Mission Planner GCS, one of the 3DR 915 MHz telemetry radios was plugged into the APM 2.8, as shown in Figure 21, while a second telemetry radio

was connected to a PC using an USB cable. Since we have the communication link between two telemetry radios, we can check the link status in terms of the number of transmitted packets, frequency range, number of channels and  $T_x$  power (shown in Figure 22a).

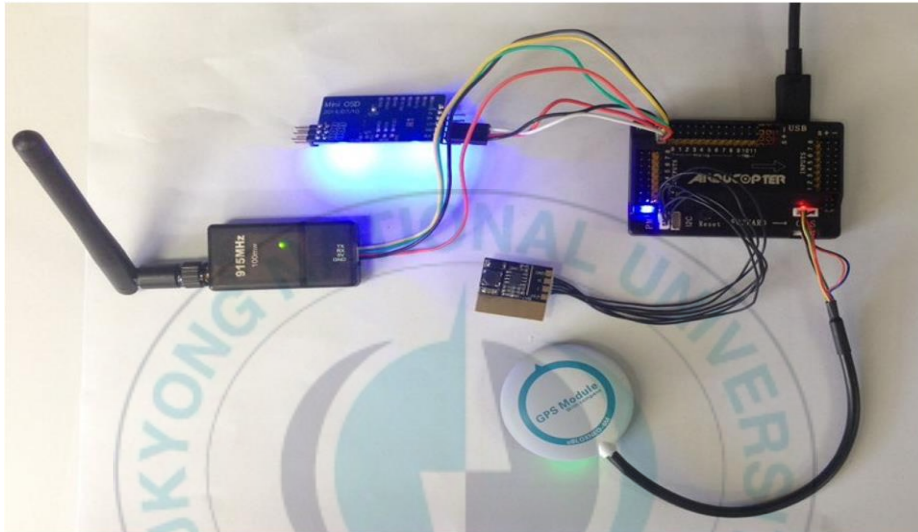
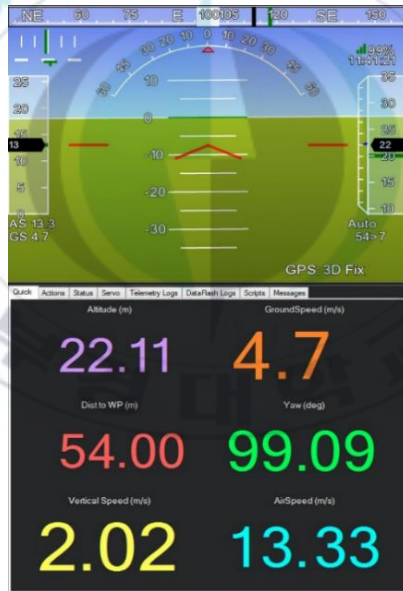


**Fig. 21.** Layout of experimental setup.

We configured the connection settings using Mission Planner. After establishing a successful connection, the telemetry data were obtained from the GCS. It should be noted that these data can be represented as signals when they are carried by the MAVLink through wireless link between the APM 2.8 and GCS. All relevant information about APM 2.8 such as altitude, yaw, pitch, roll, attitude, vertical speed, ground speed, etc., are shown in the “Flight Data” screen of the Mission Planner (see Figure 22b). When we move the APM 2.8 microcontroller from one place to another, “Flight Data” screen will display the telemetry data according to the new position of APM 2.8. Afterwards, the telemetry data collected from the GCS were imported into the MATLAB for the modulation process.



(a)



(b)

**Fig. 22.** Mission Planner GCS: (a) Radio link status; (b) “Flight Data” screen.

In order to perform the modulation process in MATLAB, we have used the data that were gathered from the GCS and static simulation parameters shown in Table 4.

**Table 4.** Simulation parameters.

Parameter	Value
System bandwidth	10 MHz
Frequency	2.4 GHz
Modulation scheme	BPSK, QPSK, 8-PSK, 16-QAM, 64-QAM
Number of subcarriers	1024
Data block size	32
Cyclic prefix	64
Pulse shaping filter	Raised-cosine (RC) / Root raised-cosine (RRC)
Roll-off factor	0.3
Oversampling factor	5
Number of iterations	$10^4$
Subcarrier spacing	10 kHz
Equalization	Zero forcing / Minimum mean square error (MMSE)

The input data symbols  $x_n$  for  $0 \leq n \leq N - 1$  are modulated by one of the modulation schemes using an  $N$ -point DFT to generate a representation of the frequency domain of the input symbols and then, the SC-FDM output sequence  $X_k$  for  $0 \leq k \leq N - 1$  is given by:

$$X_k = \sum_{n=0}^{N-1} x_n e^{-j\frac{2\pi nk}{N}}, \quad 0 \leq k \leq N - 1. \quad (5)$$

The SC-FDM symbol  $X[k]$  is a complex number that consists of real and imaginary parts. According to the central limit theorem, as the number of subcarriers  $N$  gets larger, the real and imaginary parts of the SC-FDM symbols follow the normal (Gaussian) distribution and the probability density function (PDF) of  $X[k]$  can be shown as [32]:

$$f_{X_k}(x) = \frac{x}{\sigma^2} e^{\frac{-x^2}{2\sigma^2}}, \quad (6)$$

where  $\sigma$  is the standard deviation.

### 3.2.2.2 *Peak-to-Average Power Ratio (PAPR)*

One of the key parameters for analyzing the performance of the transferred signal is its peak-to-average power ratio (PAPR), which indicates how extreme the peaks are in a waveform. This can be determined as the ratio of peak power to the average power of the transmitted signal [39]. In a multicarrier system, PAPR occurs when the different subcarriers do not correspond to a phase with each other at each point. It means that these subcarriers are different relative to each other for different phase values. The value of PAPR depends on the number of subcarriers involved as well as on the modulation scheme. It should be mentioned that high PAPR requires a high power consumption for transmitting a signal. In other words, it can be said that the efficiency of the power amplifier will be very low. On the other hand, a lower value of PAPR results in an increase in the flight time (battery life) of the vehicle. The PAPR of the transmitted signal is defined in the units of dB and it can be expressed as follows:

$$PAPR_{dB} = 10 \log_{10} \left( \frac{|X_{max}|^2}{X_{ms}^2} \right), \quad (7)$$

where  $X_{max}$  is the maximum value and  $X_{ms}$  is the mean square value of the signal. Here, PAPR is equivalent to the crest factor, as it is defined in decibels. Now, if we consider that  $X_{max}$  denotes the crest factor, it can be written by:

$$X_{max} = \max_{k=0,1,\dots,N-1} X_k. \quad (8)$$

The cumulative distribution function (CDF) of  $X_{max}$  is the probability that  $X_{max}$  will take a value less than or equal to  $x$ . The CDF of  $X_{max}$  is described by [40]:

$$\begin{aligned} F_{X_{max}}(x) &= P(X_{max} \leq x) \\ &= \int_0^x f_{Y_k}(y) dy \end{aligned} \quad (9)$$

$$\begin{aligned} &= \int_0^x \frac{y}{\sigma^2} e^{\frac{-y^2}{2\sigma^2}} dy, \\ CDF &= 1 - e^{\frac{-x^2}{2\sigma^2}}. \end{aligned} \quad (10)$$

Since we have the Equations (9) and (10), we can characterize the PAPR by using a complementary cumulative distribution function (CCDF). The CCDF of the PAPR is the probability of the PAPR which is higher than a certain PAPR value and it can be calculated as:

$$\begin{aligned} CCDF &= 1 - P(PAPR \leq x) \\ &= 1 - \left(1 - e^{\frac{-x^2}{2\sigma^2}}\right)^N. \end{aligned} \quad (11)$$

### 3.2.2.3 Bit Error Rate (BER)

Another important parameter for measuring the performance of a wireless channel of a UAV communication system is the bit error rate (BER). When data is

transmitted over a wireless link between the vehicle and GCS, the BER specifies the number of errors that appear in the received data. The environmental conditions and changes to the propagation path are the fundamental reasons for the communication channel degradation and the respective BER.

To achieve an acceptable BER, i.e., for the transmission of control commands on uplink, typical acceptable BER is around  $10^{-6}$ - $10^{-9}$ , while that acceptable value for the transmission of payload data on downlink is  $10^{-3}$ - $10^{-4}$  [41], all the available factors must be balanced. Usually, it is difficult to achieve all the requirements and some compromises are required. Moreover, a higher level of error correction is needed in order to recover the original data. This can help to fix the effects of any occurred bit error. It results to the fact that the overall BER can be improved. If the bidirectional communication between the transmitter and receiver is established very well and the signal-to-noise ratio (SNR) is high, then the BER will be potentially insignificant and will not have an observable effect on the whole UAV communication system. The BER is equal to the number of bit errors ( $N_E$ ) divided by the total number of transmitted bits ( $N_T$ ), as expressed by the following equation:

$$BER = \frac{N_E}{N_T}. \quad (12)$$

The  $N_E$  can be computed by comparing the transmitted signal with the received signal. The BER is most often expressed in terms of SNR. The SNR can be defined as the ratio of bit energy ( $E_b$ ) to the noise power spectral density ( $N_o$ ), which is a power per Hz and it is expressed as follows:

$$SNR = \frac{E_b}{N_o}, \quad (13)$$

where  $E_b$  is a measure of energy and can be defined by dividing the carrier power by the bit rate.

The probability of bit error ( $P_b$ ) represents the probability that the error rate arises in the received signal. The  $P_b$  for M-ary PSK can be defined as:

$$P_b \cong 2Q \left[ \sqrt{\frac{2E_{av}}{N_o}} \sin\left(\frac{\pi}{M}\right) \right], \quad (14)$$

where  $E_{av}$  is the average energy of transmitted symbol.  $Q$  represents the scaled form of the complementary error function (erfc) and it is given by:

$$Q(x) = \frac{1}{2} \operatorname{erfc}\left(\frac{x}{\sqrt{2}}\right). \quad (15)$$

It is necessary to note that each different kind of modulation scheme has its own value for the error function. This is due to the fact that each type of modulation scheme executes in different ways in the presence of noise.

Finally, we can calculate the  $P_b$  for M-ary QAM by using the following equation:

$$P_b \cong 4 \left(1 - \frac{1}{\sqrt{M}}\right) Q \left[ \sqrt{\frac{3E_{av}}{(M-1)N_o}} \right]. \quad (16)$$

#### 3.2.2.4 Pulse Shaping

The pulse shaping can be used to make the transmitted signal more suitable for the communication channel. In general, pulse shaping is important to ensure the

correspondence of a signal in its frequency band. In this paper, raised-cosine (RC) and root raised-cosine (RRC) pulse shaping filters are used to get the desired spectrum. To perform the frequency response of the RC filter, we use the following equation:

$$H_{RC}(f) = \begin{cases} T, & 0 \leq |f| \leq \frac{1-\alpha}{2T} \\ \frac{T}{2} \left\{ 1 + \cos \left[ \frac{\pi T}{\alpha} \left( |f| - \frac{1-\alpha}{2T} \right) \right] \right\}, & \frac{1-\alpha}{2T} \leq |f| \leq \frac{1+\alpha}{2T} \\ 0, & \text{otherwise} \end{cases} \quad (17)$$

where  $f$  is the frequency,  $T$  is the symbol period and  $\alpha$  is the roll-off factor and its value can be between 0 and 1. The representation of the time domain of this filter is given by:

$$h_{RC}(t) = \frac{\sin\left(\frac{\pi t}{T}\right) \cos\frac{\pi \alpha t}{T}}{\frac{\pi t}{T} \left[ 1 - \left(\frac{2\alpha t}{T}\right)^2 \right]}, \quad (18)$$

where  $t$  is the time. Equations (17) and (18) are used to realize the frequency and impulse responses of the RC filter. Then, the frequency domain transfer function of the RRC filter can be written as:

$$G_{RRC}(f) = \sqrt{H_{RC}(f)}. \quad (19)$$

The impulse response of the RRC filter is given by:

$$g_{RRC}(t) = \frac{\sin\left(\frac{\pi t}{T}(1 - \alpha)\right) + \frac{4\alpha t}{T} \cos\left(\frac{\pi t}{T}(1 + \alpha)\right)}{\frac{\pi t}{T} \left[1 - \left(\frac{4\alpha t}{T}\right)^2\right]}. \quad (20)$$

Finally, the performance of each modulation scheme for SC-FDM and OFDM can be measured by calculating the different values of the above mentioned parameters. To achieve the comparative results that are presented in the following section, the simulation parameters and the data that were collected from the GCS were utilized as the inputs of the system performed with MATLAB.

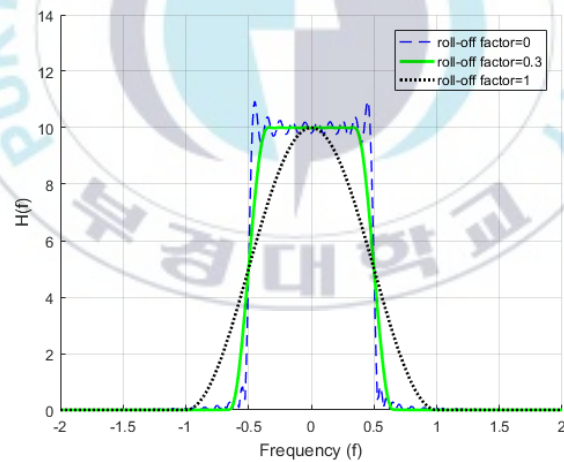
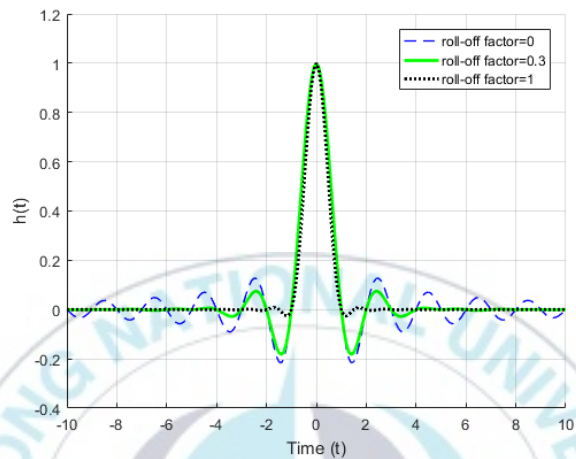
### 3.2.3 Results Analysis

In this work, MATLAB was used to perform the PAPR simulations of SC-FDM and OFDM as well as the probability of bit error simulation for SC-FDM using different kinds of modulation schemes such as BPSK, QPSK, 8-PSK, 16-QAM and 64-QAM. Of course, it is essential to select the optimal number of subcarriers, types of the pulse shaping filters and channel equalization when simulation parameters are inputted. The number of subcarriers and symbols depends on the cyclic prefix and the subcarrier spacing.

#### 3.2.3.1 *The Impulse and Frequency Responses of the Raised-Cosine (RC) filter*

When RC and RRC pulse shaping filters are used to filter a symbol stream, they can minimize an ISI. Half of this filtering can be done on the transmitter and second half can be done on the receiver. The impulse and frequency responses of the RC filter based on different roll-off factors have been plotted and shown in Figure 23. Furthermore, the equalizer can be used to get the recovery of the transmit symbols by reducing an ISI. By removing all ISI, the zero forcing equalizer can be the optimal choice in the noiseless channel. On the other hand, when channel is noisy, this equalizer significantly amplifies the noise at frequencies. In this case, minimum

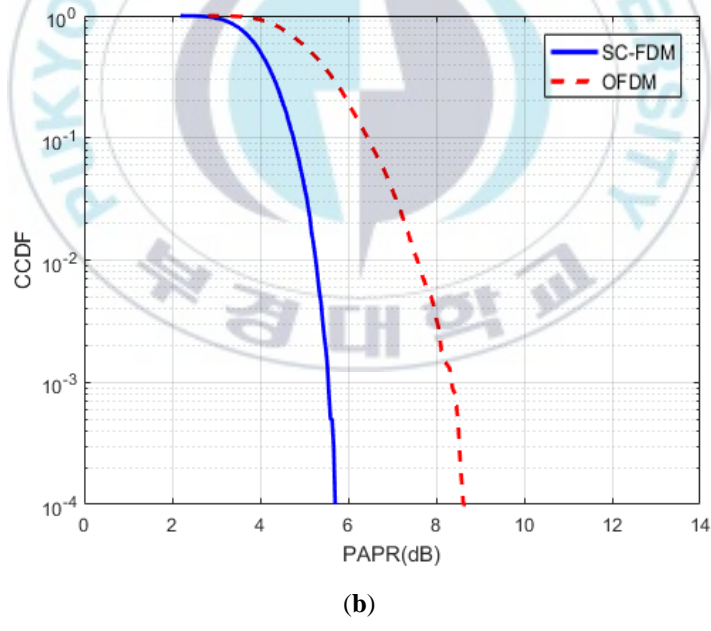
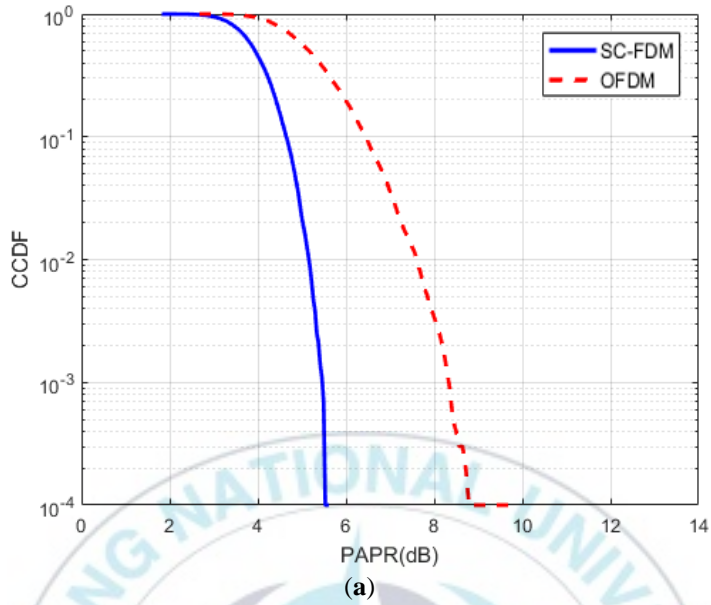
mean square error (MMSE) equalizer can be more efficient than zero forcing. The main function of MMSE equalizer is minimizing the ISI components and entire power of the noise in the output instead of eliminating ISI completely.

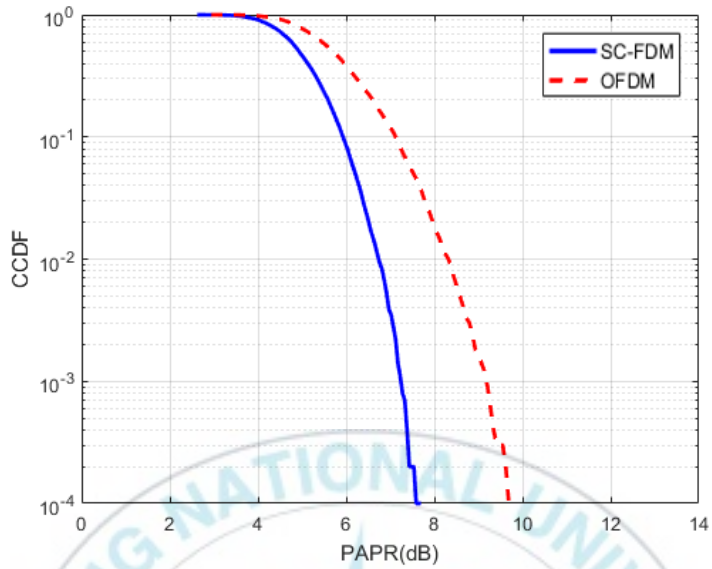


**Fig. 23.** The impulse and frequency responses of the RC filter: (a) The impulse response; (b) The frequency response.

### 3.2.3.2 PAPR Results

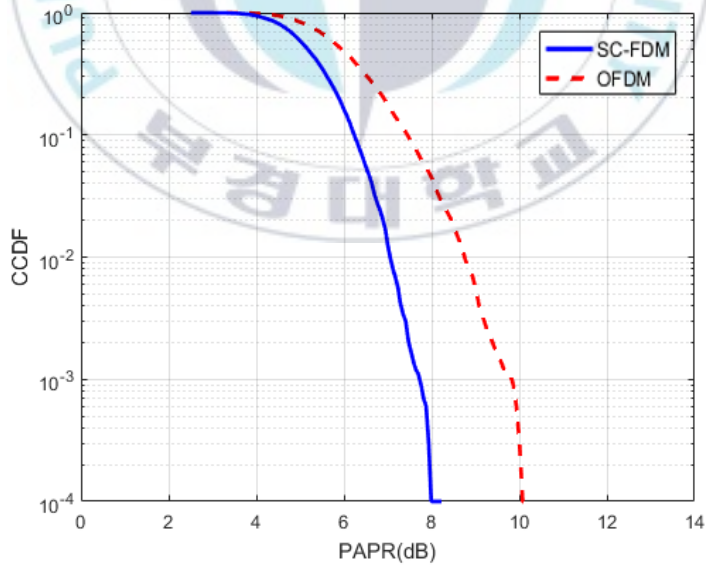
Figures 24 and 25 plot the peak-to-average power ratio (PAPR) measurements of SC-FDM and OFDM against the complementary cumulative distribution function (CCDF). According to the simulation results, which are shown in Figures 24 and 25, the SC-FDM has an advantage over OFDM because of its lower PAPR that leads to an increase in battery performance for a UAV. As shown in Figure 24(a, b), it can be seen that the PAPR value of SC-FDM for BPSK modulation scheme (5.6 dB) is almost same as that for QPSK (5.7 dB) when the CCDF is  $10^{-4}$ . At the same point, PAPR value of OFDM for BPSK is 8.8 dB and, for QPSK, it equals to 8.6 dB. In addition, the simulation results show that 8-PSK has slightly lower PAPR value than 16-QAM for both SC-FDM and OFDM. From Figure 25, it can be observed that increasing the order of QAM modulation scheme (16-QAM and 64-QAM) results in growing up the PAPR values of SC-FDM and OFDM from 8 dB and 10 dB to 10 dB and 12.2 dB, respectively. From Figures 24 and 25, we can conclude that the abrupt change in the CCDF value comes from the fact that PAPR values are expressed in logarithmic scale for both SC-FDM and OFDM modulation techniques. The PAPR values of SC-FDM and OFDM for different modulation schemes are presented in Table 5.



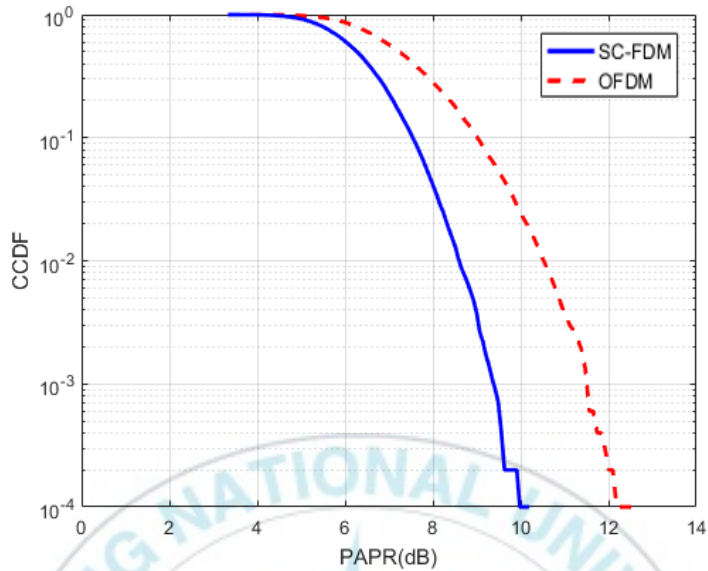


(c)

**Fig. 24.** The PAPR performances of SC-FDM and OFDM for M-ary PSK modulation schemes: (a) BPSK; (b) QPSK; (c) 8-PSK.



(a)



(b)

**Fig. 25.** The PAPR performances of SC-FDM and OFDM for M-ary QAM modulation schemes: (a) 16-QAM; (b) 64-QAM.

**Table 5.** PAPR results for SC-FDM and OFDM.

Modulation Scheme	PAPR (dB)	
	SC-FDM	OFDM
BPSK	5.6	8.8
QPSK	5.7	8.6
8-PSK	7.6	9.7
16-QAM	8	10
64-QAM	10	12.2

### 3.2.3.3 The Probability of Bit Error Results

The probability of bit error of different modulation schemes for SC-FDM is shown in Figure 26. From this figure, we can observe that the BPSK and QPSK modulation schemes achieve better performances than other modulation schemes. It is obvious

that BPSK and QPSK modulation schemes are very suitable for SC-FDM modulation technique, according to their PAPR and the probability of bit error performances (see Table 5 and Figure 26).

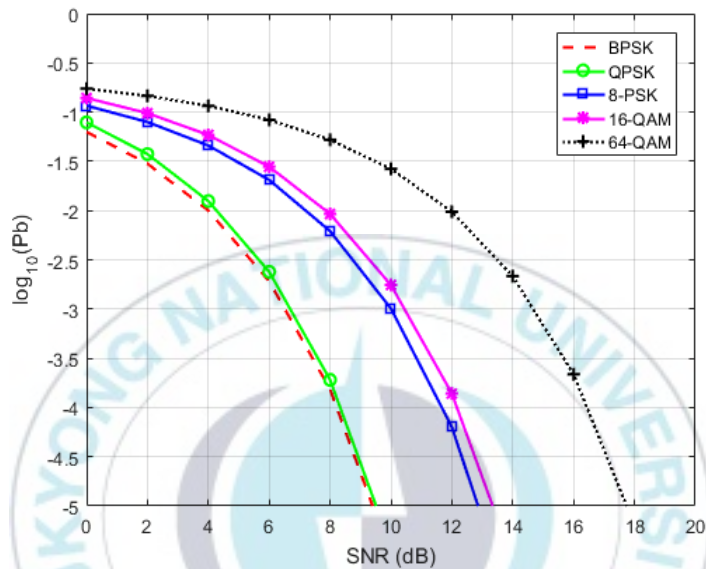


**Fig. 26.** The probability of bit error of different modulation schemes for SC-FDM modulation technique.

In this work, in order to evaluate the complexity of the proposed framework in term of computation time, we used a computer with Inter(R) Core(TM) i7-4790 CPU 3.60 GHz; RAM: 16.0 GB; Operating System: Windows 8.1 Pro 64-bit and MATLAB R2016a. As demonstrated in Figure 27, the computation time of SC-FDM and OFDM modulation techniques depends on the number of subcarriers.

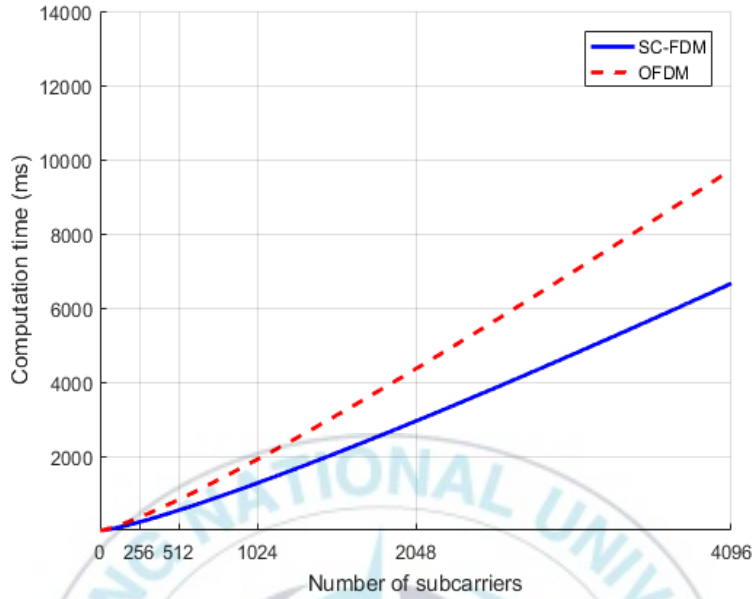


**Fig. 27.** Computation time comparison of SC-FDM and OFDM.

In Table 6, we have shown the computation time of SC-FDM and OFDM modulation techniques. The computation time of SC-FDM is ranged from 222 to 6653 ms with  $|N| \in [256, 4096]$ , while the range for OFDM is between 350 and 9723 ms. We can conclude that the computation time of SC-FDM is lower than the one of OFDM.

**Table 6.** Computation time for SC-FDM and OFDM.

Number of subcarriers	Computation Time (ms)	
	SC-FDM	OFDM
256	222	350
512	542	829
1024	1278	1916
2048	2941	4348
4096	6653	9723

## IV. Conclusion

In general, this thesis is divided into two parts. In the first part of our work, the MAVLink communication protocol has been analyzed and a method to secure a communication link between the Unmanned Aerial Vehicle (UAV) and Ground Control Station (GCS) has been provided. For this purpose, APM 2.8 board was tested to analyze a data link between the GCS and autopilot using Mission Planner and Wireshark softwares. In order to secure a communication link, AES-128 encryption algorithm is selected because of its security level and speed of encryption.

In the second part, we have analyzed the SC-FDM modulation technique in order to provide an efficient communication link between the vehicle and GCS, since the communication link is an essential part of the UAV. The main purpose of this work was to analyze the SC-FDM modulation technique by comparing it with the OFDM. The comparative results obtained by using various types of modulation schemes such as BPSK, QPSK, 8-PSK, 16-QAM and 64-QAM show that SC-FDM is more effective than OFDM for the UAV communication system, leading to a noticeable improvement in terms of efficiency of the UAV communication link and flight time of quadcopters. Moreover, by analyzing the results of our work, we have found that BPSK and QPSK are optimal modulation schemes for SC-FDM modulation technique.

Due to the fact that currently used 2.4 GHz band for a UAV communication link is utilized by many different communication systems leading to generate the interferences, some drones have already been designed to operate in the 5.8 GHz band. Thus, our further work will focus on analyzing the 5.8 GHz band for a UAV communication system.

## References

- [1] D. Ehichioya and A. Golriz, "Performance Comparison of OFDM and DSSS on Aeronautical Channels," *Proceedings of the 45th International Telemetry Conference*, Las Vegas, Nevada, USA, 26-29 October 2009.
- [2] K.P. Valavanis and G.J. Vachtsevanos, "UAV Applications: Introduction," *Handbook of Unmanned Aerial Vehicles*, Springer, Dordrecht, 2017, pp. 2639–2641.
- [3] P.G. Fahlstrom and T.J. Gleason, *Introduction to UAV Systems*, 4th ed., John Wiley & Sons, 2012.
- [4] S. Atoev, K.R. Kwon, S.H. Lee, and K.S. Moon, "Data Analysis of the MAVLink Communication Protocol," *Proceedings of the IEEE International Conference on Information Science and Communications Technologies (ICISCT)*, Tashkent, Uzbekistan, 2-4 November 2017.
- [5] S. Atoev, O.H. Kwon, S.H. Lee, and K.R. Kwon, "An Efficient SC-FDM Modulation Technique for a UAV Communication Link," *Electronics Journal*, Vol. 7, Issue 12, 2018.
- [6] A. Bosso, C. Conficoni, and A. Tilli, "Multirotor UAV flight endurance and control: The drive perspective," *Proceedings of the 42nd Annual Conference of the IEEE Industrial Electronics Society (IECON 2016)*, Florence, Italy, 23-26 October 2016; pp. 1839–1845.
- [7] A.O. Kuzmenko, "Optimal Choice of Technical Means of UAV Communication Link," *Proceedings of the IEEE 3rd International Conference on Actual Problems of Unmanned Aerial Vehicles Developments (APUAVD)*, Kyiv, Ukraine, 13-15 October 2015; pp. 149–152.
- [8] Z. Wu, H. Kumar, and A. Davari, "Performance Evaluation of OFDM Transmission in UAV Wireless Communication," *Proceedings of the 37th*

- Southeastern Symposium on System Theory (SSST)*, Tuskegee, AL, USA, 20-22 March 2005; pp. 6–10.
- [9] G. Miko and A. Nemeth, “SCFDMA based communication system for UAV applications,” *Proceedings of the 25th International Conference Radioelektronika*, Pardubice, Czech Republic, 21-22 April 2015; pp. 222–224.
- [10] H.G. Myung, J. Lim, and D.J. Goodman, “Single Carrier FDMA for Uplink Wireless Transmission” *IEEE Vehic. Tech. Mag.*, Vol. 1, pp. 30-38, 2006.
- [11] S.B. Lande, J.D. Gawali, and S.M. Kharad, “Performance Evolution of SC-FDMA for Mobile Communication System,” *Proceedings of the 5th International Conference on Communication Systems and Network Technologies (CSNT)*, Gwalior, MP, India, 4-6 April 2015; pp. 416–420.
- [12] P.A. Thomas and M. Mathurakani, “Effects of Different modulation schemes in PAPR reduction of SC-FDMA System for Uplink Communication,” *International Journal of Advan. Res. Elect. Electron. Instrum. Eng.*, Vol. 3, pp. 8531-8539, 2014.
- [13] N. Kaur and N. Gupta, “Simulation and Analysis of OFDM and SC-FDMA with STBC using Different Modulation Techniques,” *International Journal of Advan. Res. Comp. Eng. Tech.*, Vol. 4, pp. 4184-4189, 2015.
- [14] Z. Luo and X. Xiong, “Performance Comparison of SC-FDMA-CDMA and OFDM-CDMA Systems for Uplink,” *Proceedings of the International Conference on Consumer Electronics, Communications and Networks (CECNet)*, Xianning, China, 16-18 April 2011; pp. 1475–1479.
- [15] X. Xiong and Z. Luo, “SC-FDMA-IDMA: A Hybrid Multiple Access Scheme for LTE Uplink,” *Proceedings of the 7th International Conference on Wireless Communications, Networking and Mobile Computing (WiCOM)*, Wuhan, China, 23-25 September 2011.

- [16] H.G. Myung, "Introduction to Single Carrier FDMA," *Proceedings of the 15th European Signal Processing Conference (EUSIPCO)*, Poznan, Poland, 3-7 September 2007; pp. 2144–2148.
- [17] J.J. Ahmed, "PAPR Reduction of Localized Single Carrier FDMA using Partial Transmit Sequence in LTE Systems," *International Journal of Com. Net. Tech.*, Vol. 5, pp. 21-26, 2017.
- [18] M.M. Rana, J. Kim, and W.K. Cho, "Performance analysis of subcarrier mapping in LTE uplink systems," *Proceedings of the 9th International Conference on Optical Internet (COIN)*, Jeju, South Korea, 11-14 July 2010.
- [19] E.E. Tsiropoulou, A. Kapoukakis, and S. Papavassiliou, "Energy-efficient Subcarrier Allocation in SC-FDMA Wireless Networks based on Multilateral Model of Bargaining," *Proceedings of the 2013 IFIP Networking Conference*, Brooklyn, NY, USA, 22-24 May 2013; pp. 1–9.
- [20] E.E. Tsiropoulou, I. Ziras, and S. Papavassiliou, "Service Differentiation and Resource Allocation in SC-FDMA Wireless Networks through User-Centric Distributed Non-Cooperative Multilateral Bargaining," *Proceedings of the International Conference on Ad Hoc Networks (ADHOCNETS)*, San Remo, Italy, 1-2 September 2015; pp. 42–54.
- [21] E.E. Tsiropoulou, A. Kapoukakis, and S. Papavassiliou, "Uplink resource allocation in SC-FDMA wireless networks: A survey and taxonomy," *Journal of Comp. Net.*, Vol. 96, pp. 1-28, 2016.
- [22] Z. Luo and X. Xiong, "Analysis of the Effect of Carrier Frequency Offsets on the performance of SC-FDMA-IDMA Systems," *Proceedings of the 2nd International Conference on Consumer Electronics, Communications and Networks (CECNet)*, Yichang, China, 21-23 April 2012; pp. 889–893.
- [23] G. Crespo, G.G. Rivera, J. Garrido, and R. Ponticelli, "Setup of a communication and control systems of a quadrotor type Unmanned Aerial

- Vehicle,” *Proceedings of the 29th Conference on Design of Circuits and Integrated Systems (DCIS)*, Madrid, Spain, 26-28 November 2014.
- [24] B. Li, “Study on Modeling of Communication Channel of UAV,” *Journal of Proc. Comp. Sci.*, Vol. 107, pp. 550-557, 2017.
- [25] J. Ma and H. Liu, “Performance Analysis and Simulation of UAV Data Link and Communication Link,” *Proceedings of the International Conference on Network, Communication, Computer Engineering (NCCE)*, Chongqing, China, 26-27 May 2018.
- [26] J. Li, Y. Ding, and Z. Fang, “Key Techniques Research on UAV Data Link,” *Journal of Proc. Eng.*, Vol. 99, pp. 1099-1107, 2015.
- [27] E. Petritoli, F. Leccese, and L. Ciani, “Reliability and Maintenance Analysis of Unmanned Aerial Vehicles,” *Sensors Journal*, Vol. 18, 2018.
- [28] A. Lidbom and E. Kiniklis, “Providence – UAV support for search and rescue,” *M.S. Thesis, Dept. of Signals and Systems, Chalmers University of Technology*, Gothenburg, Sweden, 2015.
- [29] M. Mozaffari, W. Saad, M. Bennis, and M. Debbah, “Unmanned Aerial Vehicle with Underlaid Device-to-Device Communications: Performance and Tradeoffs,” *IEEE Trans. Wir. Com.*, Vol. 15, pp. 3949-3963, 2016.
- [30] E. Kalantari, H. Yanikomeroglu, and A. Yongacoglu, “On the Number and 3D Placement of Drone Base Stations in Wireless Cellular Networks,” *Proceedings of the IEEE 84th Vehicular Technology Conference (VTC-Fall)*, Montreal, QC, Canada, 18-21 September 2016.
- [31] M. Mozaffari, W. Saad, M. Bennis, and M. Debbah, “Efficient Deployment of Multiple Unmanned Aerial Vehicles for Optimal Wireless Coverage,” *IEEE Com. Let.*, Vol. 20, pp. 1647-1650, 2016.
- [32] S. Ramavath and R.S. Kshetrimayum, “Analytical calculations of CCDF for some common PAPR reduction techniques in OFDM systems,” *Proceedings of the IEEE International Conference on Communications, Devices and*

- Intelligent Systems (CODIS)*, Kolkata, India, 28-29 December 2012; pp. 405–408.
- [33] LTE Uplink and SC-FDMA. Available online: [https://www.exploreagate.com/Video.aspx?video\\_id=55](https://www.exploreagate.com/Video.aspx?video_id=55) (accessed on 4 September 2018).
- [34] F. Kristensen, P. Nilsson, and A. Olsson, “A Generic Transmitter for Wireless OFDM Systems,” *Proceedings of the IEEE 14th Conference on Personal, Indoor and Mobile Radio Communications (PIMRC)*, Beijing, China, 7-10 September 2003; pp. 2234–2238.
- [35] M. Rumney, “3GPP LTE: Introducing Single-Carrier FDMA,” *Technical Report, Agilent Technologies*, January 2008.
- [36] H. Nigam and M.K. Patidar, “Performance Evaluation of CFO in Single Carrier-FDMA,” *International Journal of Elect. Electron. Comp. Eng.*, Vol. 3, pp. 104-110, 2014.
- [37] I. Girdhar, C. Singh, and A. Kumar, “Performance Analysis of DFT Spread OFDM Systems,” *International Journal of Advan. Comp. Sci. Tech.*, Vol. 2, pp. 21-26, 2013.
- [38] MAVLink Protocol Overview. Available online: <https://mavlink.io/en/protocol/overview.html> (accessed on 15 September 2018).
- [39] M.F. Pervej, M.Z.I. Sarkar, T.K. Roy, and M.N.Y. Koli, “Impact Analysis of Input and Output Block Size of DCT-SCFDMA System,” *Proceedings of the IEEE 17th International Conference on Computer and Information Technology (ICCIT)*, Dhaka, Bangladesh, 22-23 December 2014; pp. 440–445.
- [40] Y.S. Cho, J. Kim, W.Y. Yang, and C.G. Kang, *MIMO-OFDM Wireless Communications with MATLAB*, John Wiley & Sons (Asia) Pte Ltd: 2 Clementi Loop, #02-01, Singapore, 2010.

- [41] S. Baiotti, G.L. Scazzola, G. Battaini, and E. Crovari, "Advances in UAV Data Links: Analysis of Requirement evolution and implications of future equipment," *Proceedings of the RTO SCI Symposium on Warfare Automation: Procedures and Techniques for Unmanned Vehicles*, Ankara, Turkey, 26-28 April 1999.
- [42] N. Pramstaller, F.K. Gurkaynak, S. Haene, H. Kaeslin, N. Felber, and W. Fichtner, "Towards an AES crypto-chip resistant to differential power analysis," *Proceedings of the 30th European Solid-State Circuits Conference (ESSCIRC)*, Leuven, Belgium, 21-23 September 2004.



## Acknowledgement

This thesis would not have been completed without the supports and help from people around me. First of all, I would like to thank my advisor, **Prof. Ki-Ryong Kwon**, for the patient guidance, encouragement and advice he has provided throughout my time as his student. I have been extremely lucky to have an advisor who cared so much about my work, and who responded to my questions and queries so promptly. I am so grateful for his endless help and care what he has given to me. I would also like to thank my co-advisors, **Prof. Suk-Hwan Lee** and **Prof. Oh-Heum Kwon**, for their useful comments and suggestions that helped me to revise this thesis.

Furthermore, I would also like to express my sincere gratitude to my lab seniors: **Dr. Jin-Hyeok Park**, **Dr. Pham Ngoc Giao**, **Dr. Caleb Bruce Vununu Ngandu** and **Mr. Nguyen Viet Hoan**; also my lab mates: **Ms. Thanh Thi Phuong Tran**, **Mr. Rafiul Hasan Khan**, **Mr. Min-Kyu Song**, **Mr. Khurshid Farkhodov** and **Mr. Long Hoang**, they gave me lots of useful suggestions and comments, experience, knowledge, and helped me in difficult situations during the study period. Moreover, I am very grateful to all the students from Uzbekistan at PKNU with whom I have had the pleasure to study here in Busan.

Finally, it should be noted that nobody has been more important to me in the pursuit of graduate studies than the members of my family. I would like to thank my parents, whose love and guidance are with me in whatever I pursue. Most importantly, I would like to thank my loving and supportive wife, who has provided endless inspiration.